PNAS RESEARCH ARTICLE | CELL BIOLOGY

IFT80 negatively regulates osteoclast differentiation via association with Cbl-b to disrupt TRAF6 stabilization and activation

Vishwa Deepak[a], Shu-ting Yang[a], Ziqing Li[a], Xinhua Li[a], Andrew Ng[b], Ding Xu[b], Yi-Ping Li[c], Merry Jo Oursler[d,e], and Shuying Yang[a,f,g,1]

Edited by Mone Zaidi, Icahn School of Medicine at Mount Sinai, New York, NY; received February 1, 2022; accepted March 8, 2022 by Editorial Board Member Carl F. Nathan

Excess bone loss due to increased osteoclastogenesis is a significant clinical problem. Intraflagellar transport (IFT) proteins have been reported to regulate cell growth and differentiation. The role of IFT80, an IFT complex B protein, in osteoclasts (OCs) is completely unknown. Here, we demonstrate that deletion of IFT80 in the myeloid lineage led to increased OC formation and activity accompanied by severe bone loss in mice. IFT80 regulated OC formation by associating with Casitas B-lineage lymphoma proto-oncogene-b (Cbl-b) to promote protein stabilization and proteasomal degradation of tumor necrosis factor (TNF) receptor–associated factor 6 (TRAF6). IFT80 knockdown resulted in increased ubiquitination of Cbl-b and higher TRAF6 levels, thereby hyperactivating the receptor activator of nuclear factor-κβ (NF-κβ) ligand (RANKL) signaling axis and increased OC formation. Ectopic overexpression of IFT80 rescued osteolysis in a calvarial model of bone loss. We have thus identified a negative function of IFT80 in OCs.

osteoclast | IFT80 | bone | osteoblast

Significance

Osteoclasts (OCs) are the sole bone resorbing cells indispensable for bone remodeling. Hence, understanding of novel signaling modulators regulating OC formation is clinically important. Intraflagellar transport (IFT) proteins are important for cilia, cell signaling, and organ development. It remains unclear whether IFT80 plays a role in OCs. This study uncovers an intriguing role of IFT80 in OCs where the ciliary protein regulates the stability of critical OC factor TRAF6 via Cbl-b and thereby contributes to the maintenance of OC numbers. These findings provide further basis for understanding and delineating the role of IFT proteins in OCs that may provide new strategies for treatment of osteolytic diseases.

Osteoclasts (OCs) are giant multinucleated cells important for bone development and homeostasis. OCs differentiate from monocyte–macrophage cells of the hematopoietic lineage upon stimulation with the macrophage-colony stimulation factor (m-CSF) and receptor activator of nuclear factor-kβ (NF-κβ) ligand (RANKL) (1, 2). Excessive bone resorption owing to increased OC formation and activity is mainly responsible for the bone loss associated with diseases such as osteoporosis, Paget's disease of bone, cancer metastases to bone, and rheumatoid and osteoarthritis (3, 4). Understanding of osteoclastogenic mechanisms is clinically important for treatment of bone loss diseases.

Intraflagellar transport (IFT) proteins aid in bidirectional movement of multisubunit protein particles along the axonemal microtubules and ciliary assembly (5), which are essential for ciliary assembly and function (5). However, a growing body of evidence now indicates that ciliary proteins are also present at nonciliary sites and perform distinct functions other than those needed in cilia (6, 7).

Lymphoid cells such as T cells are considered to lack cilia, and IFT20, one of the IFT-B groups of proteins, has been reported to regulate immune synapse polarization (8). IFT80 is also an IFT-B protein (9). In humans, mutations in IFT80 cause Jeune syndrome and short-rib polydactyly type III (10, 11) with severe bone phenotypes such as narrow chest, short ribs, shortened bones, and polydactyly. Our previous reports have shown that IFT proteins are important for regulation of osteoblasts (OBs), chondrocyte-dependent skeletal maintenance, polarity and cell alignment, and T cell development (12–15). However, the role and mechanism of IFT80 in OCs are completely unknown.

c-Casitas B lineage lymphoma (c-Cbl) and Casitas B lineage lymphoma-b proto-oncogene-b (Cbl-b) are two homologous proteins that act as ubiquitin ligases and are reported to modulate innate immune responses and play key roles in host defense and antitumor immunity (16). Cbl proteins are expressed in hematopoietic cells and OCs (17). c-Cbl primarily regulates OC podosomes and motility, and a bone phenotype is not detectable in c-Cbl–knockout mice (18). On the other hand, Cbl-b–devoid mice have a pronounced bone phenotype with increased OC numbers (17). However, the exact molecular mechanism by which Cbl-b regulates OC formation is incompletely understood. Tumor necrosis factor (TNF) receptor–associated factor 6 (TRAF6) is a critical upstream mediator of RANKL signaling (19). Binding of RANKL to RANK triggers a signaling cascade that involves recruitment of the adaptor molecule TRAF6 that is indispensable for activation of nuclear factor-κB (NF-κβ), mitogen-activated protein kinase (MAPK), and nuclear factor of activated t cells 1 (NFATc1) pathways (20). TRAF6-knockout mice are completely devoid of OCs with osteopetrosis phenotype (19). Recently, c-Cbl was shown to regulate TRAF6 proteasomal degradation;

Author contributions: S.Y. designed research; V.D., S.-t.Y., Z.L., X.L., A.N., and D.X. performed research; S.Y. contributed new reagents/analytic tools; V.D. and S.Y. analyzed data; and V.D., S.-t.Y., Y.-P.L., M.J.O., and S.Y. wrote the paper.

The authors declare no competing interest.

This article is a PNAS Direct Submission. M.Z. is a guest editor invited by the Editorial Board.

Copyright © 2022 the Author(s). Published by PNAS. This article is distributed under Creative Commons Attribution-NonCommercial-NoDerivatives License 4.0 (CC BY-NC-ND).

[1]To whom correspondence may be addressed. Email: shuyingy@upenn.edu.

This article contains supporting information online at http://www.pnas.org/lookup/suppl/doi:10.1073/pnas.2201490119/-/DCSupplemental.

Published June 21, 2022.

Downloaded from https://www.pnas.org by TULANE UNIVERSITY RUDOLPH MATAS MED LIBRARY on June 23, 2022 from IP address 129.81.255.98.

however, the possibility that Cbl-b has a role in TRAF6 degradation during OC formation was not explored (21).

In this study, we analyzed the role of Cbl proteins in regulation of OC formation downstream of IFT80. We conditionally deleted IFT80 in OC precursors via lysozyme M–Cre (LysM-Cre) and in mature OCs via the cathepsin K–Cre (Ctsk-Cre) mouse model (22). Ablation of IFT80 caused increased OC differentiation and bone loss in mice. Interestingly, we further found that IFT80 associated with Cbl-b and TRAF6. Deletion of IFT80 dampened the IFT80–Cbl-b–TRAF6 association and impaired the degradation of TRAF6 by Cbl-b but not by c-Cbl, causing sustained activation of RANKL signaling and increased OC numbers. Thus, our study reveals that IFT80 is an essential negative regulator in OC differentiation through controlling ubiquitination of Cbl-b and TRAF6 degradation.

Results

Loss of IFT80 in OC Precursors Significantly Decreased Bone Mass in Mice. To delineate the role of IFT80, we first analyzed the protein expression levels of IFT80 in OCs. Protein levels of IFT80 were higher in OCs than bone marrow macrophages (BMMs) (Fig. 1*A*). To further characterize the role of this protein in OCs, we generated IFT80 conditional knockout (IFT80$^{d/d}$ cKO) mice in the myeloid lineage by using a LysM-Cre mouse model. Efficient deletion of IFT80 in IFT80$^{d/d}$ cells was confirmed by Western blot (Fig. 1*B*). Microcomputed tomography (μCT) imaging showed significant bone loss (4-fold) in 12-wk-old IFT80$^{d/d}$ mice (Fig. 1*C*) compared with the LysM-Cre control mice. Increased numbers of TRAP+ OCs (1.7-fold) were present in the bone sections of 3-mo-old IFT80$^{d/d}$ mice compared with those in the control bone samples (Fig. 1*D*). Bone histomorphometry observations (Fig. 1 *E*–*G*) and serum procollagen type 1 amino-terminal propeptide (P1NP) levels (indicative of bone formation) (Fig. 1*H*) showed no significant difference between the control and IFT80$^{d/d}$ mice. Serum C-telopeptide of type I collagen (CTX-1) levels (indicative of bone resorption) were significantly higher in IFT80$^{d/d}$ mice than in control mice (Fig. 1*I*). RANKL-to-Osteoprotegerin (OPG) ratios were not significantly different between IFT80$^{d/d}$ and control mice (Fig. 1 *J*–*L*). These results indicated that deletion of IFT80 increased OC formation and activity.

IFT80 Negatively Regulates OC Differentiation and Function. To further characterize whether the increased bone loss observed in IFT80$^{d/d}$ mice occurred due to a direct effect of IFT80 on OC numbers or activity, we performed ex vivo OC differentiation and activity experiments. BMMs were isolated from IFT80$^{d/d}$ and control LysM-Cre mice to study OC differentiation and function. Ex vivo OC differentiation assay from BMMs revealed a 2.7-fold increase in TRAP+ OC formation of the IFT80$^{d/d}$ groups compared with that of the LysM-Cre group (Fig. 2*A*). BMMs derived from IFT80-ablated mice differentiated into OCs in a dose-responsive manner (*SI Appendix*, Fig. S1). OCs derived from the IFT80$^{d/d}$ group were larger in size and had consistently increased nuclear numbers (>10 nuclei; 4-fold) than the control group, which readily formed smaller OCs (Fig. 2*A*). In ex vivo coculture of wild-type (WT) OBs with OCs from LysM-Cre and IFT80$^{d/d}$ BMMs, IFT80$^{d/d}$ BMMs formed OCs that were ∼3-fold higher in number than the OCs derived from LysM-Cre BMMs (Fig. 2*B*), suggesting the introduction of OBs cannot rescue the enhanced OC differentiation caused by IFT80 deletion. To determine the effect of IFT80 on OC function, we performed acridine orange assays and actin ring assays. The results showed that IFT80$^{d/d}$ OCs displayed higher acid content (1.8-fold) (Fig. 2*C*). Furthermore,

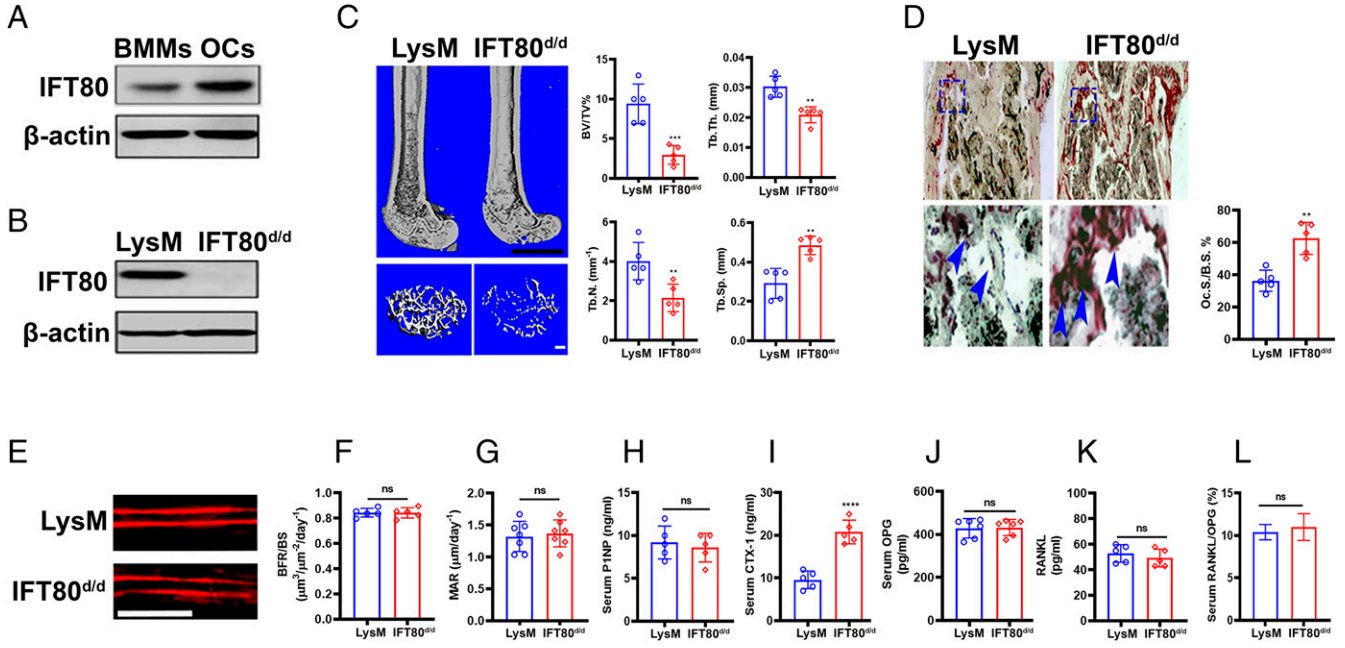

Fig. 1. LysM-Cre IFT80 cKO mice are osteopenic. (*A*) Representative Western blot image demonstrating protein expression of IFT80 (80 kDa) in BMMs and OCs ($n = 5$). (*B*) Representative Western blot image demonstrating deletion of IFT80 ($n = 5$); β-actin (43 kDa). (*C*) μCT analysis of the femurs from 12-wk-old control and IFT80$^{d/d}$ mice. (Scale bars, 1 mm.) Quantitative analysis of the percentage of bone volume over total volume (BV/TV), trabecular thickness (Tb.Th), trabecular number (Tb.N), and trabecular spacing (Tb.Sp) in the femurs of 12-wk-old control and cKO mice ($n = 5$). (*D*) Histological sections of tibiae from 12-wk-old control and IFT80$^{d/d}$ mice stained for TRAP (red) ($n = 5$). (*D*, *Lower*) Images represent enlarged views. Blue arrowheads represent OCs derived from the blue dotted boxes (*Upper*). Oc.S/B.S., osteoclast surface/bone surface ($n = 5$). (*E*–*G*) Calcein labeling in 12-wk-old LysM and IFT80$^{d/d}$ mice assessed using nondecalcified frozen sections of trabecular bone (*E*) and its quantification (*F* and *G*) (BFR, bone formation rate; MAR, mineral apposition rate) ($n = 5$). (Scale bar, 100 μm.) (*H*) Serum P1NP levels ($n = 5$). (*I*) Serum CTX-1 levels ($n = 5$). (*J*–*L*) Serum OPG (*J*), RANKL (*K*), and OPG-to-RANKL ratio (*L*) ($n = 5$). Results are expressed as mean ± SD. Data were analyzed using unpaired two-tailed *t* test. $^{**}P < 0.01$, $^{***}P < 0.001$, $^{****}P < 0.0001$. ns, nonsignificant.

Downloaded from https://www.pnas.org by TULANE UNIVERSITY RUDOLPH MATAS MED LIBRARY on June 23, 2022 from IP address 129.81.255.98.

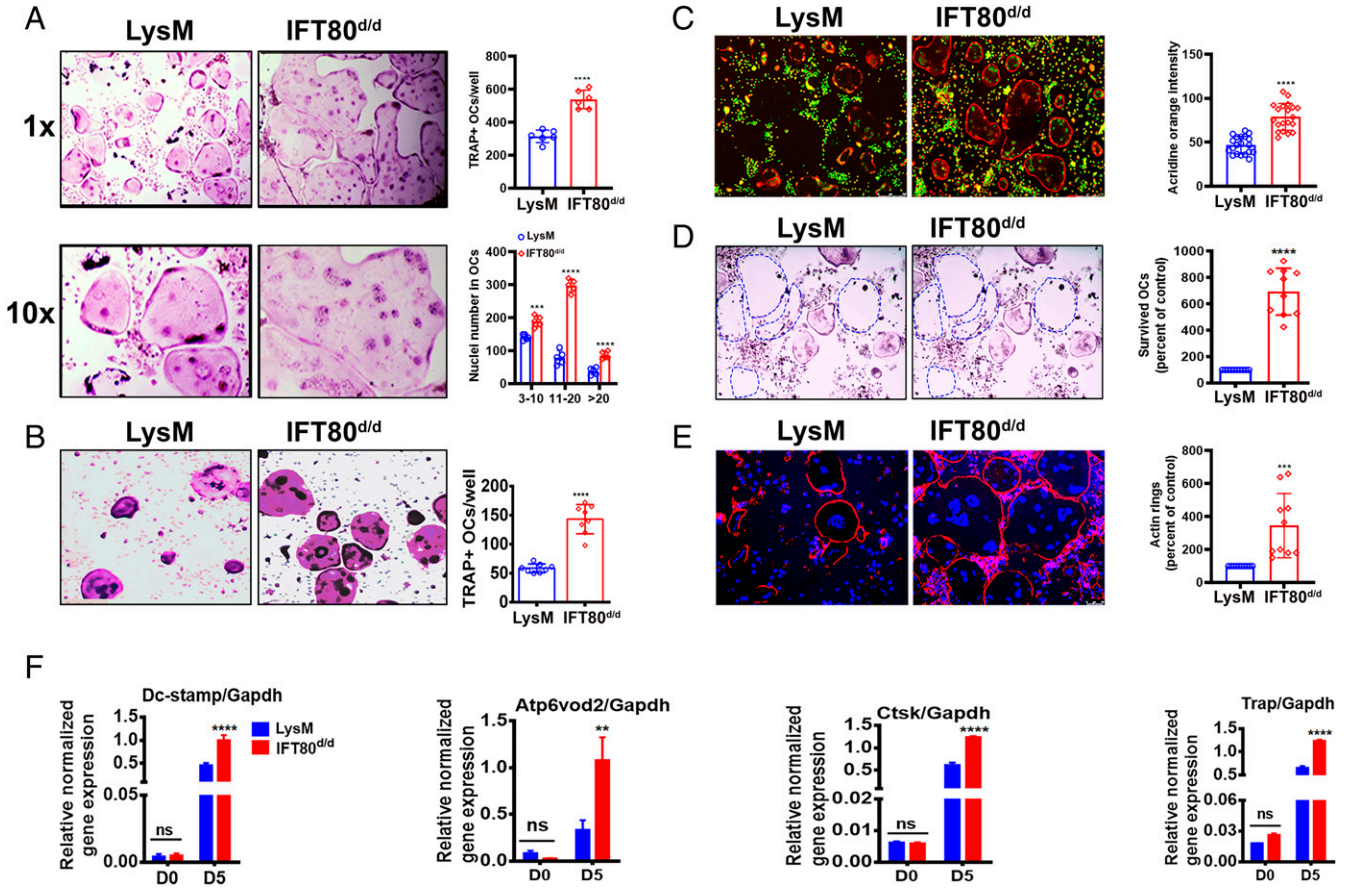

Fig. 2. Ablation of IFT80 increases OC differentiation. BMMs obtained from the long bones of LysM-Cre or IFT80$^{d/d}$ mice were differentiated into OCs for 5 d. (*A*) Number of TRAP+ stained OCs or nuclei number in OCs (n = 10). (*A*, *Lower*) Tenfold enlarged images. (*B*) OB/OC coculture model demonstrating increased differentiation of OCs (TRAP+) in the IFT80$^{d/d}$ group cultured with WT OBs (n = 8). (*C*) Increased acidification as seen by acridine orange staining (n = 20). (*D*) TRAP+ staining to detect OC survival rate at day 8 (n = 10) (blue dotted lines indicate impressions of OCs that were present earlier). (*E*) Actin ring formation analyzed by phalloidin staining (n = 10). (*F*) qRT-PCR analyses of OC-specific genes in LysM and IFT80$^{d/d}$ samples (n = 3). Results are expressed as mean ± SD. Data were analyzed either using unpaired two-tailed t test or one- or two-way ANOVA as appropriate followed by Bonferroni post hoc test. $^{**}P < 0.01$, $^{***}P < 0.001$, $^{****}P < 0.0001$. ns, nonsignificant.

IFT80$^{d/d}$ OCs showed a 6-fold increase in survival rate compared with LysM-Cre OCs when cultured for a prolonged duration (8 d) (Fig. 2*D*). Additionally, mutant OCs displayed a 3-fold increase in intact actin ring numbers (Fig. 2*E*). Moreover, messenger RNA (mRNA) levels of genes involved in OC fusion, dendrocyte-expressed seven-transmembrane protein (Dc-stamp) (23), ATPase H+-transporting V0 subunit d2 (Atp6v0d2) (24), and proteases involved in matrix dissolution, tartrate-resistant acid phosphatase (TRAP) (25), and Ctsk (26) were more increased in IFT80$^{d/d}$ OCs than in control cells (Fig. 2*F*). To investigate whether deletion of IFT80 affects myeloid cell populations, we conducted flow cytometry analysis of BMMs from LysM-Cre control and IFT80$^{d/d}$ mice. We found that LysM-Cre–mediated deletion of IFT80 did not lead to changes in the percentage of different cell populations of myeloid cells as compared with WT cells (*SI Appendix*, Fig. S2*A*). Additionally, RANK receptor expression was also comparable in both groups (*SI Appendix*, Fig. S2*B*). Viability or proliferation of the precursor cells was unaffected by IFT80 deletion (*SI Appendix*, Fig. S3). These results further indicated that IFT80 negatively regulates OC differentiation and ablation of IFT80 promotes OC formation.

Deletion of IFT80 in Mature OCs Increases OC Number and Bone Loss. Given that deletion of IFT80 in OC precursors via LysM-Cre led to increased OC numbers and bone loss, we further analyzed the effects of IFT80 deletion in mature OCs by the Ctsk-Cre mouse model (Fig. 3*A*). Ctsk-Cre–mediated IFT80-knockout mice showed significant bone loss, with a 7-fold decrease in bone volume to total bone volume (BV/TV) compared with the control mice (Fig. 3*B*). IFT80-deleted mice had a 4-fold increase in the numbers of TRAP+ OCs in the bone sections compared with bone samples in the control mice (Fig. 3*C*). BMMs obtained from Ctsk-Cre; IFT80$^{d/d}$ mice differentiated in higher numbers than the control mice (2.3-fold), with increased numbers of intact actin rings (3-fold) and acid content (1.8-fold) (Fig. 3 *D*–*F*). These results further indicated an OC-specific inhibitory role of IFT80.

Loss of IFT80 Promotes Cbl-b Ubiquitination and Impairs TRAF6 Degradation. The RANKL pathway is indispensable for OC formation (27). To further delineate whether IFT80 directly regulates the RANKL pathway, we analyzed the underlying molecular mechanisms important for regulating RANKL-mediated OC formation. As shown in *SI Appendix*, Fig. S2, flow cytometry results revealed that CD115 expression (a receptor for m-CSF; also known as c-fms) or RANK expression (a receptor for RANKL) remained unaffected after IFT80 deletion, indicating modulation in receptor expression did not occur after IFT80 ablation. TRAF6 is an upstream key adaptor molecule important for relaying RANKL signals (19, 20). Interestingly, we found that TRAF6 expression levels were dramatically increased after IFT80 deletion (Fig. 4*A*). When we ectopically overexpressed IFT80 via adenovirus in control (mock) and IFT80-deficient BMMs, we found that TRAF6

Downloaded from https://www.pnas.org by TULANE UNIVERSITY RUDOLPH MATAS MED LIBRARY on June 23, 2022 from IP address 129.81.255.98.

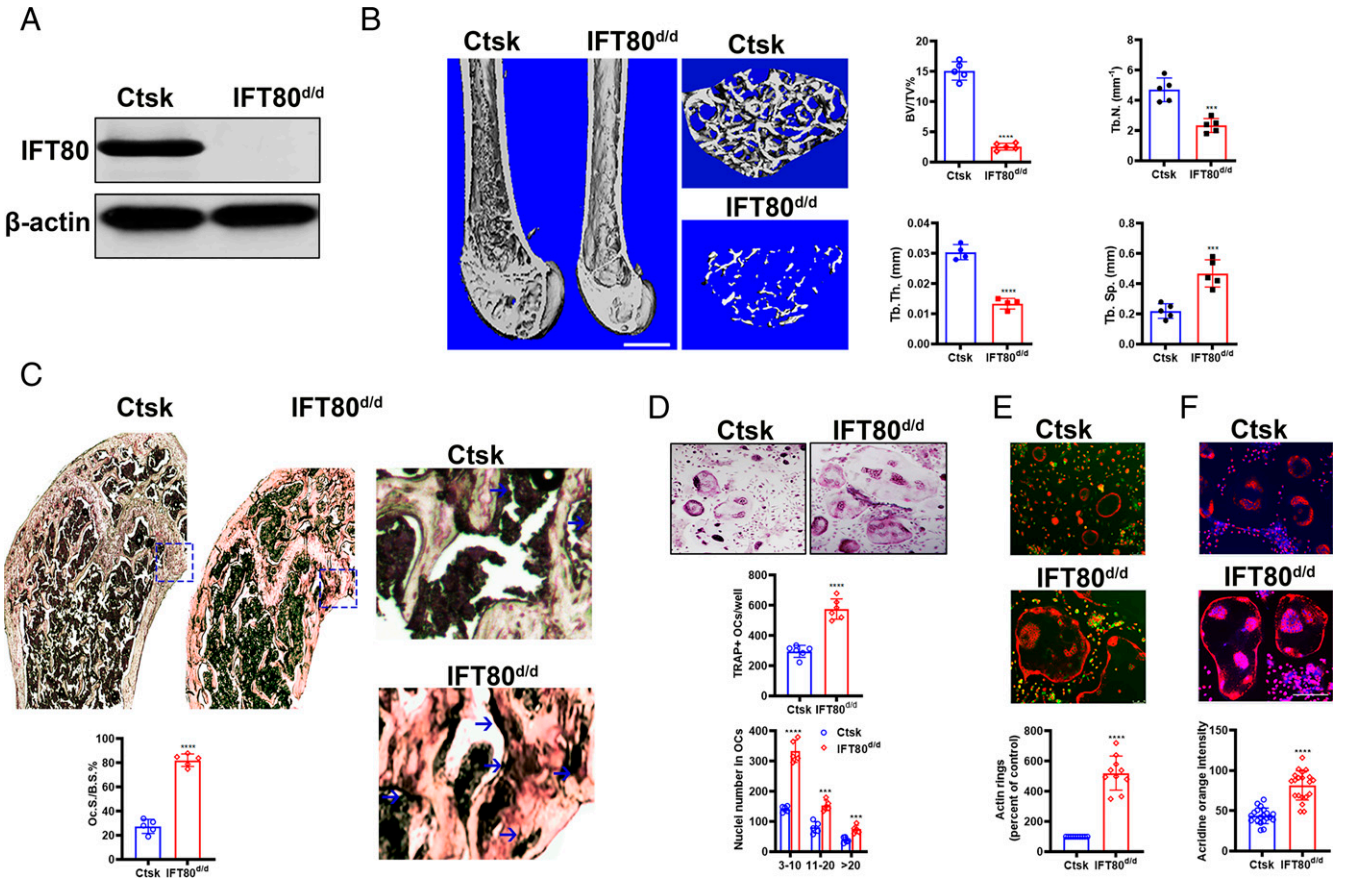

Fig. 3. Ctsk-Cre–mediated IFT80 deletion increases OC differentiation and bone loss. (*A*) Representative Western blot image demonstrating protein expression of IFT80 (80 kDa) in OCs. (*B*) μCT analysis of the femurs from 12-wk-old control and IFT80$^{d/d}$ mice ($n = 5$). (Scale bar, 50 μm.) Quantitative analysis of the percentage of BV/TV, Tb.Th, Tb.N, and Tb.Sp in the femurs of 12-wk-old control and cKO mice ($n = 5$). (*C*) Histological sections of tibiae from 12-wk-old control and IFT80$^{d/d}$ mice stained for TRAP activity (red) ($n = 5$). (*C*, *Right*) Images represent enlarged views. Blue arrows represent OCs derived from the blue dotted boxes (*Left*). Oc.S/B.S. ($n = 5$). (*D*) Number of TRAP+ stained OCs or nuclei number in OCs ($n = 6$). (*E*) Increased acidification as seen by acridine orange staining ($n = 20$). (*F*) Actin ring formation analyzed by phalloidin staining ($n = 10$). Results are expressed as mean ± SD. Data were analyzed using unpaired two-tailed *t* test. $^{**}P < 0.01$, $^{***}P < 0.001$, $^{****}P < 0.0001$.

levels were down-regulated in both groups (Fig. 4*A*). To further define whether IFT80 regulates TRAF6 protein degradation, we tested c-Cbl and Cbl-b protein levels, given that Cbl proteins are reported to regulate TRAF6 proteasomal degradation (21). Protein levels of c-Cbl and Cbl-b were up-regulated in OCs compared with those in BMMs (*SI Appendix*, Fig. S4). Interestingly, deletion or overexpression of IFT80 did not affect c-Cbl protein levels, whereas Cbl-b was up-regulated after IFT80 overexpression and reduced after IFT80 deletion (Fig. 4*A*). Overexpression of IFT80 restored Cbl-b protein levels in the IFT80$^{d/d}$ OCs (Fig. 4*A*). To find out whether IFT80 directly modulates TRAF6, we analyzed their association via coimmunoprecipitation (Co-IP). Co-IP results showed that IFT80 interacted with TRAF6 (Fig. 4*B*). Next, we analyzed whether IFT80 can promote ubiquitination and proteasomal degradation of TRAF6 via Cbl proteins. Cbl-b coimmunoprecipitated with TRAF6 and IFT80 (Fig. 4*C*) whereas c-Cbl failed to coimmunoprecipitate with IFT80 (Fig. 4*D*). Although c-Cbl was found to interact with TRAF6, this interaction was found to be independent of IFT80 presence (Fig. 4*E*). Hence, we further examined the role of Cbl-b in IFT80-mediated regulation of OC formation. Surprisingly, we found that interaction of TRAF6 with Cbl-b was dependent on the presence of IFT80 (Fig. 4*F*). Moreover, deletion of IFT80 reduced ubiquitination of TRAF6 whereas overexpression of IFT80 promoted ubiquitination of TRAF6 (Fig. 4*G*). Cbl proteins are reported to regulate themselves via autoubiquitination (28). To further find out whether the reduced levels of Cbl-b and increased protein levels of TRAF6 caused by IFT80 deficiency occur due to an effect on the ubiquitination of Cbl-b, we analyzed Cbl-b ubiquitination. Deletion of IFT80 increased ubiquitination of Cbl-b whereas overexpression of IFT80 prevented ubiquitination of Cbl-b (Fig. 4*H*). However, at these conditions, increased ubiquitination of c-Cbl was not observed in all groups (Fig. 4*I*). These results indicated that IFT80 is required for the interaction between Cbl-b and TRAF6 and loss of IFT80 promotes Cbl-b ubiquitination and thereby impairs TRAF6 degradation.

Deletion of IFT80 Hyperactivated the RANK/RANKL Signaling Axis. RANKL-induced OC differentiation involves activation of NFATc1, NF-κβ, MAPK, and PI3K/AKT pathways downstream of TRAF6 (1, 29–31). We found that deletion of IFT80 increased activation of the RANK/RANKL pathway components downstream of TRAF6 (Fig. 5*A*). Our results demonstrated that deletion of IFT80 promoted the phosphorylation of AKT, ERK1/2, and NF-κβ. Additionally, phosphorylated GSK3β, indicative of its inhibitive format (29), was also significantly increased in IFT80$^{d/d}$ BMMs (Fig. 5*A*).

To further characterize whether pharmacological inhibition of the PI3K/AKT or GSK3β signaling axis in IFT80$^{d/d}$ BMMs can perturb the increased OC differentiation effects, we used LY294002, a PI3K inhibitor (32); MK2206-HCl, an AKT inhibitor (33); and Chir99021, an inhibitor of GSK3β to treat the IFT80$^{d/d}$ and control BMMs (34). The results showed that

Downloaded from https://www.pnas.org by TULANE UNIVERSITY RUDOLPH MATAS MED LIBRARY on June 23, 2022 from IP address 129.81.255.98.

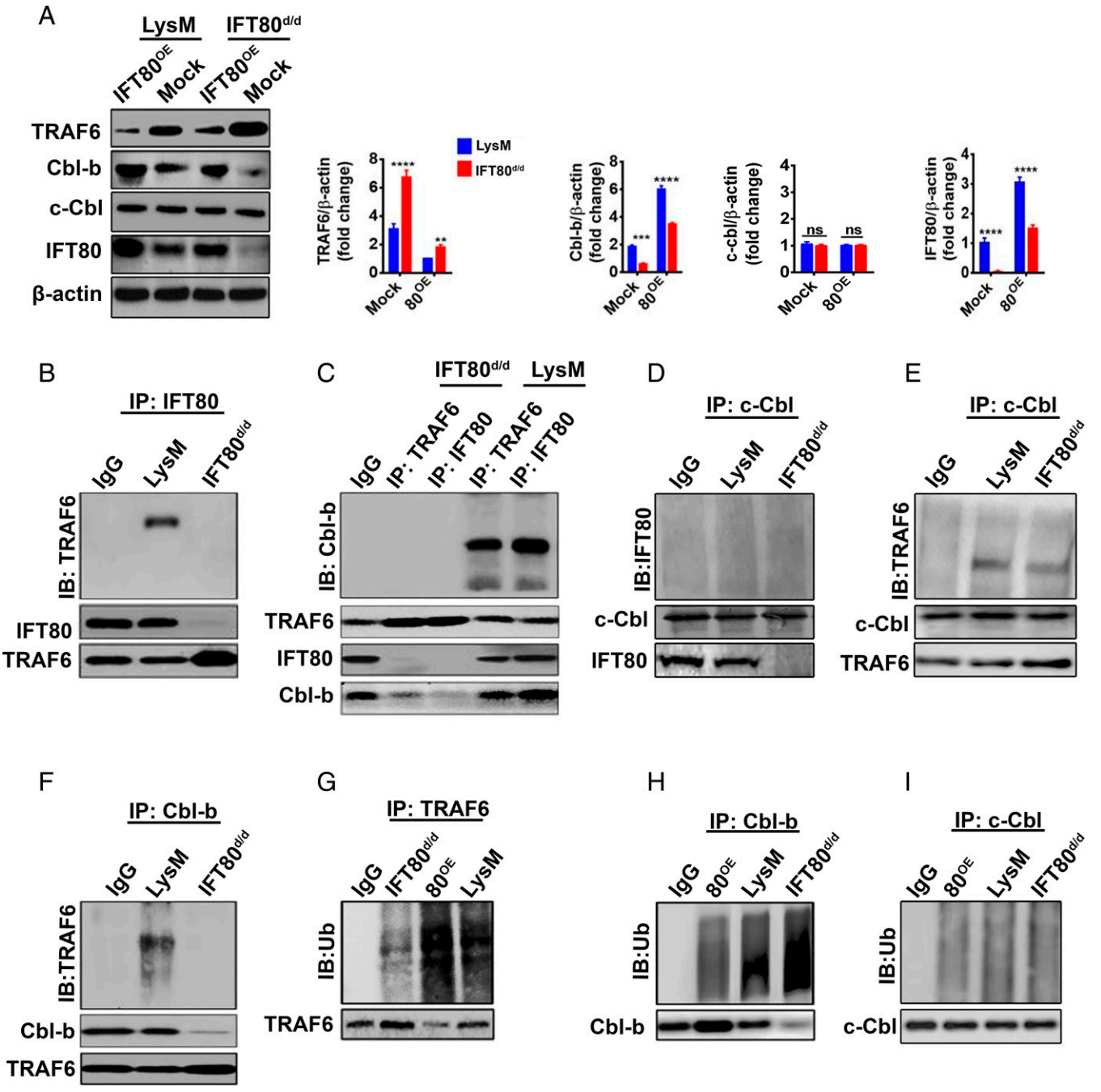

Fig. 4. IFT80 associates with TRAF6 and Cbl-b to promote TRAF6 degradation. (*A*) Protein expression of TRAF6 (molecular mass 60 kDa), Cbl-b (120 kDa), c-Cbl (105 kDa), IFT80 (80 kDa), and β-actin (43 kDa) in LysM or IFT80$^{d/d}$ BMMs with or without adenoviral overexpression of IFT80 (n = 3). Samples were stimulated with RANKL for 48 h and protein changes were analyzed by Western blot. OE in superscript denotes overexpression. Graphs represent quantification of the blots. (*B*) Co-IP of IFT80 with TRAF6 in LysM or IFT80$^{d/d}$ BMMs (n = 3). (*C*) Co-IP of TRAF6 or IFT80 with Cbl-b in LysM or IFT80$^{d/d}$ BMMs (n = 3). (*D*) Co-IP of c-Cbl with IFT80 in LysM or IFT80$^{d/d}$ BMMs (n = 3). (*E*) Co-IP of c-Cbl with TRAF6 in LysM or IFT80$^{d/d}$ BMMs (n = 3). (*F*) Co-IP of Cbl-b with TRAF6 in LysM or IFT80$^{d/d}$ BMMs (n = 3). (*G*) Co-IP of TRAF6 with Ub (ubiquitin) in LysM, IFT80$^{d/d}$, or 80^{OE} BMMs. (*H*) Co-IP of Cbl-b with Ub in IFT80$^{d/d}$, 80^{OE}, or LysM BMMs. (*I*) Co-IP of c-Cbl with Ub in IFT80$^{d/d}$, 80^{OE}, or LysM BMMs. Immunoglobulin G (IgG) was used as a nonspecific control. For the Co-IP experiments, cells were treated with RANKL for 48 h before analysis. IB, immunoblotting. Results are expressed as mean ± SD. Data were analyzed using two-way ANOVA followed by Bonferroni post hoc test. *P < 0.05, **P < 0.01, ***P < 0.001, ****P < 0.0001. ns, nonsignificant.

inhibition of PI3K or AKT pathways by these inhibitors led to a significant reduction in OC numbers in both control BMMs and IFT80$^{d/d}$ BMMs (Fig. 5*B*). GSK3β is an NFATc1-inhibitory kinase. Phosphorylation of GSK3β at Ser9 indicates inhibition of its activity that leads to release of its inhibitory effects on NFATc1. Concurrently, we found that inactivation of GSK3β by Chir99021 increased OC formation in control BMMs. Not surprisingly, no further increases in OC numbers were observed in IFT80-deficient BMMs treated with Chir99021, indicating a peak inhibition of GSK3β had already occurred after IFT80 ablation (Fig. 5*B*). At the tested concentrations, cell viability was not affected (*SI Appendix*, Fig. S5). These results indicated that IFT80 suppresses the RANKL/RANK signaling axis.

NFATc1 is an essential transcription factor for OC terminal differentiation (35). To test whether IFT80 affects NFATc1 activation, protein levels of NFATc1 in the cytoplasmic and nuclear fractions from control and IFT80$^{d/d}$ BMMs were analyzed by Western blot. IFT80$^{d/d}$ cells had higher and sustained

Downloaded from https://www.pnas.org by TULANE UNIVERSITY RUDOLPH MATAS MED LIBRARY on June 23, 2022 from IP address 129.81.255.98.

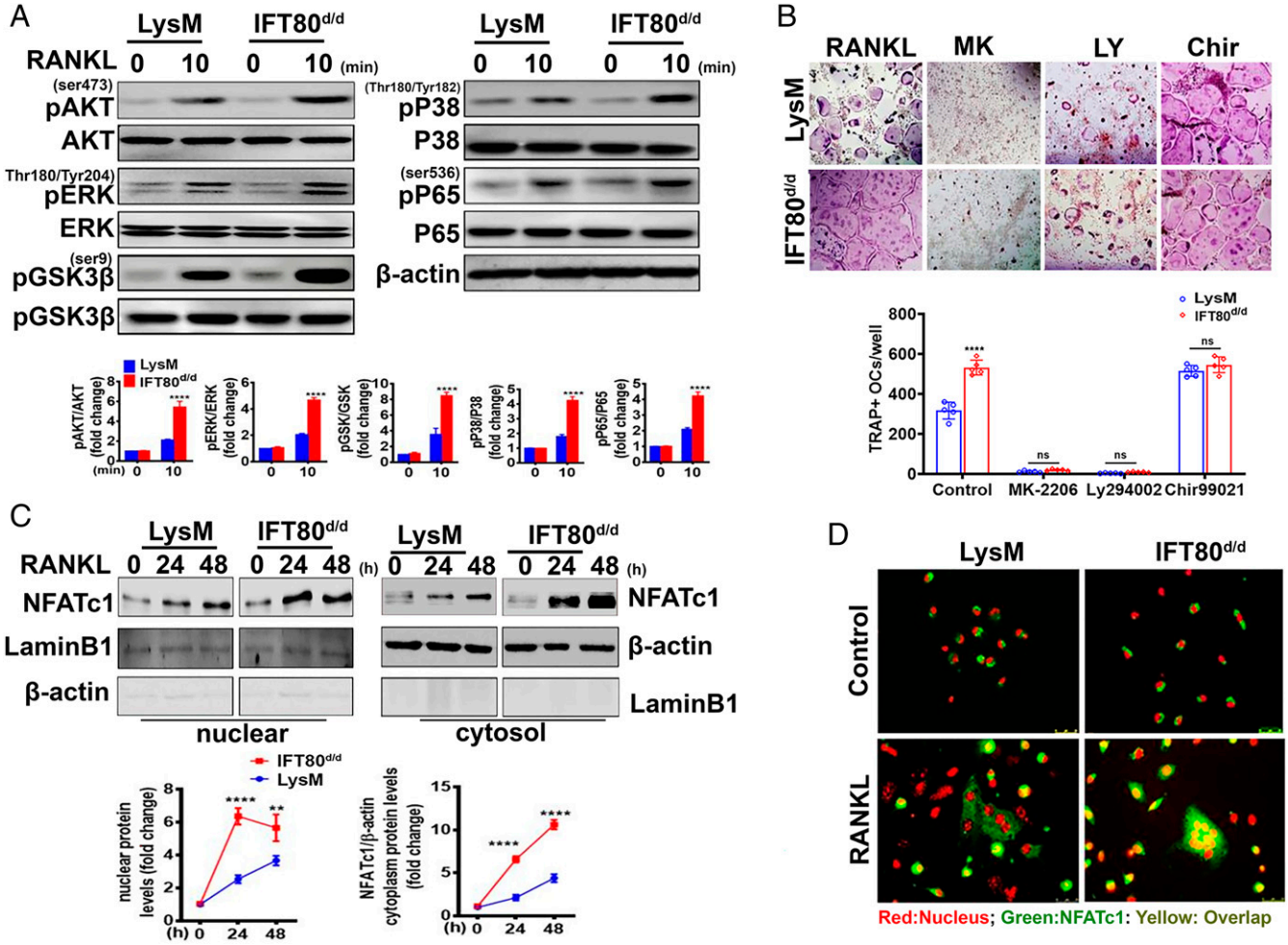

Fig. 5. IFT80 deletion hyperactivates the RANK/RANKL and downstream AKT/ERK/GSK signaling pathways. (*A*) Time-course analysis and quantification of RANKL-induced pathways by Western blot in LysM or IFT80$^{d/d}$ BMMs ($n = 3$). Graphs represent quantification of the blots. (*B*) TRAP staining and quantification of LysM and IFT80$^{d/d}$ OCs treated with MK2206-Hcl (Mk), an AKT inhibitor (0.5 μM); LY294002 (Ly), a PI3K inhibitor (1 μM); and Chir99021 (Chir), a GSK3β inhibitor (1 μM) ($n = 10$). (*C*) Western blot to analyze NFATc1 expression in nuclear and cytoplasmic fractions ($n = 3$). Graphs represent quantification of the blots. (*D*) Subcellular localization of NFATc1 was analyzed by immunofluorescence. Red, nuclei; green, NFATc1 (pseudocolored); yellow denotes overlap of red and green. Results are expressed as mean ± SD. Data were analyzed using one- or two-way ANOVA as appropriate followed by Bonferroni post hoc test. *$P < 0.05$, **$P < 0.01$, ***$P < 0.001$, ****$P < 0.0001$. ns, nonsignificant (molecular mass: pAKT/AKT: 62 kDa; pERK/ERK: 42 kDa, 44 kDa; GSK3β: 47 kDa; pP38/P38: 38 kDa; pP65/P65: 65 kDa; NFATc1: 110 kDa; LaminB1: 68 kDa; β-actin: 43 kDa).

NFATc1 nuclear and cytoplasmic levels following RANKL stimulation than control cells (Fig. 5*C*). In line with this, immunofluorescence staining results further confirmed an increase in nuclear translocation of NFATc1 protein in IFT80$^{d/d}$ BMMs as compared with the control cells (Fig. 5*D*).

Overexpression of IFT80 Suppresses Osteolysis in a RANKL-Induced Calvarial Bone Loss Mouse Model. To further elucidate whether IFT80 acts as a negative regulator for osteoclastogenesis, we analyzed whether increased expression of IFT80 could rescue bone loss. We overexpressed IFT80 in BMMs by adenovirus and analyzed its effect on OC differentiation. Interestingly, overexpression of IFT80 significantly dampened OC formation in the IFT80$^{d/d}$ group (10-fold) (Fig. 6*A*) and suppressed the RANKL/RANK downstream signaling pathways (Fig. 6*B*). To further analyze the negative effects of IFT80 under pathological conditions, we used a RANKL-induced calvarial bone loss mouse model (36). μCT results showed reduced bone volume after RANKL treatment that was rescued by 3-fold after IFT80 overexpression over the RANKL-mock group (Fig. 6*C*). These results indicated that overexpression of IFT80 reduced bone loss by suppressing increases in OC numbers.

Discussion

Primary cilia play essential roles in cell differentiation and organ formation (37). For example, deletion of ciliary genes in cells including OBs, chondrocytes, adipocytes, and myoblasts causes inhibition of cell differentiation (12, 14, 38, 39). In this study, we focused on the role of IFT80 in OCs. Our study reveals the negative regulatory functions of IFT80 in OC differentiation via association with TRAF6 and Cbl-b to promote TRAF6 degradation, thereby negatively regulating the RANKL/RANK pathway (Fig. 6*D*).

We deleted IFT80 at the early and late stages of OC differentiation using LysM-Cre (OC precursor) and Ctsk-Cre (mature OC) mouse strains. We found that IFT80-deleted mice suffered with severe bone loss in both mouse models. On the contrary, bone apposition rates remained unaffected between mutant and control mice, indicating osteopenia after the loss of IFT80. Increased numbers of OCs and activity are a common clinical manifestation in osteolytic diseases (4). Likewise, the IFT80-deficient mice had increased numbers of TRAP+ OCs in vivo and ex vivo. Mutant OCs were comparatively gigantic with an enlarged cytoplasm occupied by increased numbers of nuclei and actin rings and demonstrated

Downloaded from https://www.pnas.org by TULANE UNIVERSITY RUDOLPH MATAS MED LIBRARY on June 23, 2022 from IP address 129.81.255.98.

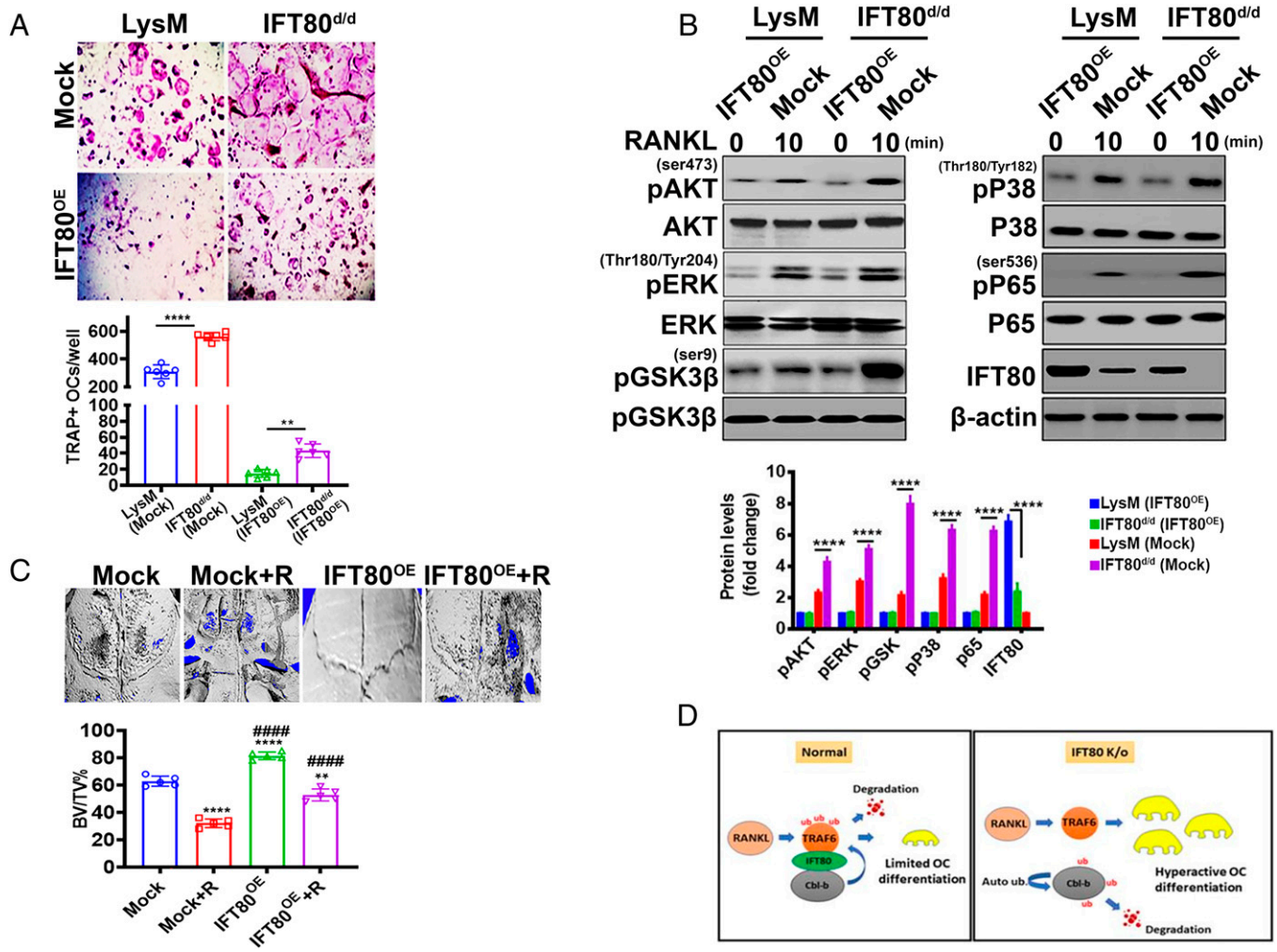

Fig. 6. Overexpression of IFT80 inhibits RANKL-induced bone lysis. (*A*) TRAP+ stained OCs and quantitative analysis in the mock and IFT80^{OE} groups (n = 3). (*B*) Time-course analysis and quantification of RANKL-induced pathways by Western blot in LysM or IFT80$^{d/d}$ BMMs with or without IFT80 overexpression (n = 3). Graphs represent quantification of the blots. $^{**}P < 0.01$, $^{****}P < 0.0001$ (molecular mass: pAKT/AKT: 62 kDa; pERK/ERK: 42 kDa, 44 kDa; GSK3β: 47 kDa; pP38/P38: 38 kDa; pP65/P65: 65 kDa; NFATc1: 140 kDa; β-actin: 43 kDa). (*C*) μCT analysis of the calvariae in mock or IFT80^{OE} mice treated with RANKL (n = 5). Quantitative analysis of the percentage of BV/TV. Results are expressed as mean ± SD. Data were analyzed using one-way ANOVA followed by Bonferroni post hoc test (n = 10). $^{####}P < 0.0001$ vs. Ad-Null + RANKL; $^{**}P < 0.01$, $^{****}P < 0.0001$ vs. control. (*D*) Schematic of the proposed mechanisms. RANKL triggers a cascade of signaling events. TRAF6 mediates the signaling pathways induced by RANKL. Under normal conditions, IFT80 bridges a link between Cbl-b and TRAF6. Cbl-b ubiquitinates TRAF6 for degradation. However, deletion of IFT80 (KO) impairs the linkage between Cbl-b and TRAF6. This likely creates a negative feedback loop, thereby promoting the autoubiquitination and degradation of Cbl-b. Absence of Cbl-b leaves TRAF6 activity unchecked, which leads to increased activation of RANK/RANKL pathways, OC numbers, and activity.

that those OCs exhibited an increased response to RANKL and had a longer life span. The mutant OCs not only had increased mRNA levels of the proteases (TRAP, Ctsk) but also had increased acid content (observed via acridine orange staining) important for bone resorption. Previously published reports suggested that increased numbers of OC precursors in diseases such as arthritis might contribute to enhanced OC formation (40). In this study, our analysis revealed that deletion of IFT80 did not affect cell percentages of myeloid precursors, thereby excluding the possibility of increased OC differentiation owing to increased progenitor populations.

RANK lacks intrinsic catalytic activity and interacts with TRAF6 that acts as an adaptor protein for activation of downstream signaling pathways (19). We found that deletion of IFT80 did not affect the expression of RANK or c-fms excluding the involvement of increased receptor activation leading to OC formation. TRAF6 modulates the effectors of RANKL signaling such as NF-κβ, MAPKs, and the PI3K axis (30, 41). Moreover, RANKL-mediated activation of TRAF6 signaling is also essential for NFATc1 induction (42). TRAF6-deficient mice show severe osteopetrosis due to impaired osteoclastogenesis and BMMs fail to differentiate ex vivo even in the presence of both m-CSF and RANKL (19). Hence, TRAF6 is a critical upstream mediator of RANKL signaling. We found that IFT80 deletion led to increased expression of TRAF6 with elevated activation of AKT, ERK, p38 MAPKs, NF-κβ, and NFATc1 and inactivation of GSK3β, critical mediators of the RANKL signaling axis. These findings are in line with previously published studies showing the NF-κβ, PI3K/AKT/GSK3β, and NFATc1 pathways act downstream of RANKL/TRAF6 and are essential for OC differentiation (29, 30, 35, 43, 44).

Our results show that the protein levels of TRAF6 are increased in the mutant cells whereas overexpression of IFT80 protein reduces TRAF6 protein level. Studies have shown that the Cbl family of ubiquitin ligases mediates the degradation of activated signaling molecules (28). Although c-Cbl–mediated TRAF6 degradation has been reported (21), it is unknown whether Cbl-b regulates TRAF6 during RANKL-mediated OC formation. In particular, the role of Cbl proteins in relation to IFT80 is unexplored hitherto. Our results demonstrate that

Downloaded from https://www.pnas.org by TULANE UNIVERSITY RUDOLPH MATAS MED LIBRARY on June 23, 2022 from IP address 129.81.255.98.

although deletion or overexpression of IFT80 significantly decreased or increased Cbl-b protein levels, respectively, an increase or decrease in IFT80 expression did not affect c-Cbl protein levels. Additionally, deletion of IFT80 decreased ubiquitination of TRAF6 and resulted in an increased ubiquitination of Cbl-b. These findings indicate that IFT80-mediated regulation of TRAF6 likely occurs via Cbl-b. These results are further supported by previous findings from Baron and coworkers that loss of Cbl-b increases OC activity and induces osteopenia in mice (17) and c-Cbl and Cbl-b perform unique functions in OCs that cannot be compensated by the other homolog. It has been shown that c-Cbl primarily regulates OC structure and motility, whereas Cbl-b is involved in regulating OC numbers (17). The functions for both Cbl proteins are redundant in OC podosome formation and survival. These findings indicated that redundancy shared by the c-Cbl and Cbl-b proteins is to regulate OC motility and survival (45). Of note, the exact molecular mechanisms regulated by Cbl-b in OC formation is not understood, especially in relation to the role of IFT80 protein. By further studying the relationship between IFT80, TRAF6, and Cbl-b, we found that IFT80 can interact with TRAF6 and Cbl-b. Notwithstanding, this interaction between TRAF6 and Cbl-b is dependent on IFT80, as Cbl-b failed to associate with TRAF6 in IFT80-deleted conditions. These results suggest that IFT80 bridges a link between these proteins. The TRAF6/IFT80/Cbl-b signaling ensures that the OC differentiation occurs in a regulated manner and thereby prevents excessive bone resorption. Loss of IFT80 creates a negative feedback loop where Cbl-b–mediated degradation of TRAF6 is impaired, causing ubiquitination and degradation of Cbl-b. This leads to an unchecked activation of TRAF6 signaling causing enhanced OC formation and activity.

In summary, we provide evidence that IFT80 links TRAF6 and Cbl-b signaling to negatively regulate OC differentiation. These findings not only further our understanding of the fundamentals of OC cell biology but also reveal mechanisms for understanding the complex molecular pathways regulating OC formation.

Methods

Antibodies. A detailed list of antibodies is provided in *SI Appendix*.

Mice. The LysM-Cre (22) mice were purchased from the Jackson Laboratory. Ctsk-Cre mice and IFT80$^{flox/flox}$ mice have been described previously (13, 46, 47). Mice carrying the IFT80^{flox} allele were crossed with either LysM-Cre or Ctsk-Cre mice to generate IFT80$^{d/d}$ mice. Three-month-old mice were used throughout the study unless stated otherwise. All animal studies were approved by the Institutional Animal Care and Use Committee at the University of Pennsylvania.

Radiographic and Histologic Analysis. For three-dimensional μCT analyses, samples were prepared as described earlier on a μCT 35 (Scanco) (46). Detailed information is provided in *SI Appendix*.

Histomorphometric Analyses. Dynamic histomorphometry was performed by double calcein labeling in 12-wk-old mice. Detailed information has been provided in *SI Appendix*.

OC Differentiation. OCs were differentiated from BMMs and TRAP was stained as described previously (27, 48). Detailed information has been provided in *SI Appendix*.

Coculture of OBs and OCs. OBs were isolated from calvaria of neonate WT C57BL/J mice as described previously (49). For OB/OC coculture, BMMs were seeded on top of the calvarial OBs in the presence of 1,25-dihydroxy vitamin D3 (10 nM) and dexamethasone (10 nM) and differentiated for 7 d (50).

Serum Assays. Serum was collected via terminal bleeds from all mice. Soluble RANKL and OPG in blood plasma were measured using the mouse PicoKine Kit (BosterBio) according to the manual provided by the manufacturer. The serum levels of a bone formation marker, P1NP, and a bone resorption marker, CTX-1, were quantified using enzyme-linked immunosorbent assay kits from Immunodiagnostic Systems as described by the manufacturer.

NFATc1 Subcellular Localization Analysis. BMMs isolated from LysM-cre or IFT80 cKO mice were treated with RANKL for 3 d and stained with NFATc1 antibody. Nuclei were stained with DAPI.

Actin Ring Assay and Acridine Orange Assay. OC actin rings were stained with fluorescein isothiocyanate–phalloidin. Acid production was determined using acridine orange as described previously (51). Acridine orange intensity was quantified using LAS X software (Leica).

IFT80 Adenoviral Overexpression and RANKL-Induced Calvarial Bone Loss Model. Ad-IFT80 (IFT80^{OE}) and Ad-Null (mock) adenoviruses obtained from Vector Biolabs were injected over the midline of the mouse calvariae. Detailed information has been provided in *SI Appendix*.

Flow Cytometry to Determine Populations of Progenitor Cells in the Bone Marrow. BMMs from 2-mo-old mice were harvested for single-cell suspensions and subjected to flow cytometry analysis. Detailed information has been provided in *SI Appendix*.

Gene Expression Analyses. Total RNA was isolated using TRIzol (Thermo Fisher) according to the manufacturer's instructions. First-strand complementary DNAs (cDNAs) were synthesized using the PrimeScript cDNA Synthesis Kit (Takara). qPCR analysis was performed with the CFX96 Real-Time PCR Detection System (Bio-Rad Laboratories) using SYBR Green Master Mix (Bimake). Primer sequences used are mentioned in *SI Appendix*, Table S1.

Western Blot Analysis. Western blots were performed using routinely used methods as described earlier (46). More information is provided in *SI Appendix*.

Coimmunoprecipitation. Co-IP was performed as described earlier with brief modifications (52). Detailed information is provided in *SI Appendix*. Total protein was extracted by cell lysis in Pierce IP lysis buffer (87787) plus Halt protease/phosphatase inhibitor mixture (Thermo Scientific), followed by clearing of cell lysates through centrifugation at 14,000 × *g* for 30 min. For IP assays, the indicated antibodies were added and allowed to bind overnight at 4 °C with gentle agitation followed by incubation with protein G Plus/protein A suspension (EMD Millipore, IP05) following the manufacturer's instructions. Proteins were eluted from prewashed immunocomplexes using 2× lithium dodecyl sulfate sample buffer. Samples were subjected to Western blot. Membranes were developed with ECL reagent (SuperSignal West Femto ECL Substrate, 34094). In order to avoid intervening signals from immunoglobulin heavy and light chains, horseradish peroxidase–conjugated protein G (Bio-Rad, 1706425) was utilized.

Statistical Analysis. In each experiment, multiple mice or cell conditions were analyzed as biological replicates. A statistical analysis was performed using unpaired Student's *t* test to compare two samples or one- or two-way ANOVA ± SD followed by Bonferroni test for three or more groups. $P < 0.05$ was considered statistically significant. Samples were randomly allocated into experimental or treatment groups. The sample size for each experimental condition is indicated in the figure or corresponding figure legends. All experiments were independently repeated three or more times unless stated otherwise.

Data Availability. All study data are included in the article and/or *SI Appendix*.

ACKNOWLEDGMENTS. We acknowledge the assistance of the Penn Center for Musculoskeletal Disorders for providing access to the μCT instrument (NIH/National Institute of Arthritis and Musculoskeletal and Skin Diseases [NIAMS] P30 AR069619). Research reported in this publication was supported by the National Institute of Dental and Craniofacial Research, NIAMS, and National Institute on Aging, part of the NIH, under Awards DE023105, AR066101, and AG048388 (to S.Y.). The content is solely the responsibility of the authors and does not necessarily represent the official views of the NIH.

Downloaded from https://www.pnas.org by TULANE UNIVERSITY RUDOLPH MATAS MED LIBRARY on June 23, 2022 from IP address 129.81.255.98.

Author affiliations: [a]Department of Basic and Translational Sciences, School of Dental Medicine, University of Pennsylvania, Philadelphia, PA 19104; [b]Department of Oral Biology, School of Dental Medicine, State University of New York at Buffalo, Buffalo, NY 14214; [c]Department of Pathology and Laboratory Medicine, Tulane University School of Medicine, New Orleans, LA 70112; [d]Robert and Arlene Kogod Center on Aging, Mayo Clinic College of Medicine, Rochester, MN 55905; [e]Division of Endocrinology, Mayo Clinic College of Medicine, Rochester, MN 55905; [f]Penn Center for Musculoskeletal Disorders, School of Medicine, University of Pennsylvania, Philadelphia, PA 19104; and [g]Center for Innovation & Precision Dentistry, School of Dental Medicine and School of Engineering and Applied Sciences, University of Pennsylvania, Philadelphia, PA 19104

1. W. J. Boyle, W. S. Simonet, D. L. Lacey, Osteoclast differentiation and activation. *Nature* **423**, 337–342 (2003).
2. S. L. Teitelbaum, Bone resorption by osteoclasts. *Science* **289**, 1504–1508 (2000).
3. K. Henriksen, J. Bollerslev, V. Everts, M. A. Karsdal, Osteoclast activity and subtypes as a function of physiology and pathology–Implications for future treatments of osteoporosis. *Endocr. Rev.* **32**, 31–63 (2011).
4. H. Bi *et al.*, Key triggers of osteoclast-related diseases and available strategies for targeted therapies: A review. *Front. Med. (Lausanne)* **4**, 234 (2017).
5. L. B. Pedersen, J. L. Rosenbaum, Intraflagellar transport (IFT) role in ciliary assembly, resorption and signalling. *Curr. Top. Dev. Biol.* **85**, 23–61 (2008).
6. N. Taulet, B. Delaval, Non-ciliary functions of cilia proteins [in French]. *Med. Sci. (Paris)* **30**, 1040–1046 (2014).
7. S. Yuan, Z. Sun, Expanding horizons: Ciliary proteins reach beyond cilia. *Annu. Rev. Genet.* **47**, 353–376 (2013).
8. F. Finetti *et al.*, Intraflagellar transport is required for polarized recycling of the TCR/CD3 complex to the immune synapse. *Nat. Cell Biol.* **11**, 1332–1339 (2009).
9. A. Mourão, S. T. Christensen, E. Lorentzen, The intraflagellar transport machinery in ciliary signaling. *Curr. Opin. Struct. Biol.* **41**, 98–108 (2016).
10. P. L. Beales *et al.*, IFT80, which encodes a conserved intraflagellar transport protein, is mutated in Jeune asphyxiating thoracic dystrophy. *Nat. Genet.* **39**, 727–729 (2007).
11. D. P. Cavalcanti *et al.*, Mutation in IFT80 in a fetus with the phenotype of Verma-Naumoff provides molecular evidence for Jeune-Verma-Naumoff dysplasia spectrum. *J. Med. Genet.* **48**, 88–92 (2011).
12. X. Yuan, S. Yang, Primary cilia and intraflagellar transport proteins in bone and cartilage. *J. Dent. Res.* **95**, 1341–1349 (2016).
13. X. Yuan, L. A. Garrett-Sinha, D. Sarkar, S. Yang, Deletion of IFT20 in early stage T lymphocyte differentiation inhibits the development of collagen-induced arthritis. *Bone Res.* **2**, 14038 (2014).
14. C. Wang, X. Yuan, S. Yang, IFT80 is essential for chondrocyte differentiation by regulating Hedgehog and Wnt signaling pathways. *Exp. Cell Res.* **319**, 623–632 (2013).
15. J. Lim *et al.*, Primary cilia control cell alignment and patterning in bone development via ceramide-PKCζ-β-catenin signaling. *Commun. Biol.* **3**, 45 (2020).
16. R. Tang, W. Y. Langdon, J. Zhang, Regulation of immune responses by E3 ubiquitin ligase Cbl-b. *Cell. Immunol.* **340**, 103878 (2019).
17. A. Nakajima *et al.*, Loss of Cbl-b increases osteoclast bone-resorbing activity and induces osteopenia. *J. Bone Miner. Res.* **24**, 1162–1172 (2009).
18. R. Chiusaroli *et al.*, Deletion of the gene encoding c-Cbl alters the ability of osteoclasts to migrate, delaying resorption and ossification of cartilage during the development of long bones. *Dev. Biol.* **261**, 537–547 (2003).
19. M. A. Lomaga *et al.*, TRAF6 deficiency results in osteopetrosis and defective interleukin-1, CD40, and LPS signaling. *Genes Dev.* **13**, 1015–1024 (1999).
20. J. H. Kim, N. Kim, Signaling pathways in osteoclast differentiation. *Chonnam Med. J.* **52**, 12–17 (2016).
21. H. D. Jang, H. Z. Hwang, H. S. Kim, S. Y. Lee, C-Cbl negatively regulates TRAF6-mediated NF-κβ activation by promoting K48-linked polyubiquitination of TRAF6. *Cell. Mol. Biol. Lett.* **24**, 29 (2019).
22. B. E. Clausen, C. Burkhardt, W. Reith, R. Renkawitz, I. Förster, Conditional gene targeting in macrophages and granulocytes using LysMcre mice. *Transgenic Res.* **8**, 265–277 (1999).
23. M. Yagi *et al.*, DC-STAMP is essential for cell-cell fusion in osteoclasts and foreign body giant cells. *J. Exp. Med.* **202**, 345–351 (2005).
24. K. Kim, S. H. Lee, J. Ha Kim, Y. Choi, N. Kim, NFATc1 induces osteoclast fusion via up-regulation of Atp6v0d2 and the dendritic cell-specific transmembrane protein (DC-STAMP). *Mol. Endocrinol.* **22**, 176–185 (2008).
25. A. R. Hayman *et al.*, Mice lacking tartrate-resistant acid phosphatase (Acp 5) have disrupted endochondral ossification and mild osteopetrosis. *Development* **122**, 3151–3162 (1996).
26. B. R. Troen, The role of cathepsin K in normal bone resorption. *Drug News Perspect.* **17**, 19–28 (2004).
27. E. W. Bradley, M. J. Oursler, Osteoclast culture and resorption assays. *Methods Mol. Biol.* **455**, 19–35 (2008).
28. P. E. Ryan, G. C. Davies, M. M. Nau, S. Lipkowitz, Regulating the regulator: Negative regulation of Cbl ubiquitin ligases. *Trends Biochem. Sci.* **31**, 79–88 (2006).
29. J. B. Moon *et al.*, Akt induces osteoclast differentiation through regulating the GSK3β/NFATc1 signaling cascade. *J. Immunol.* **188**, 163–169 (2012).
30. B. R. Wong *et al.*, TRANCE, a TNF family member, activates Akt/PKB through a signaling complex involving TRAF6 and c-Src. *Mol. Cell* **4**, 1041–1049 (1999).
31. X. Feng, RANKing intracellular signaling in osteoclasts. *IUBMB Life* **57**, 389–395 (2005).
32. C. J. Vlahos, W. F. Matter, K. Y. Hui, R. F. Brown, A specific inhibitor of phosphatidylinositol 3-kinase, 2-(4-morpholinyl)-8-phenyl-4H-1-benzopyran-4-one (LY294002). *J. Biol. Chem.* **269**, 5241–5248 (1994).
33. L. Yan, Abstract #DDT01-1: MK-2206: A potent oral allosteric AKT inhibitor. *Cancer Res.* **69** (suppl. 9), DDT01-1 (2009).
34. F. Zhang, C. J. Phiel, L. Spece, N. Gurvich, P. S. Klein, Inhibitory phosphorylation of glycogen synthase kinase-3 (GSK-3) in response to lithium. Evidence for autoregulation of GSK-3. *J. Biol. Chem.* **278**, 33067–33077 (2003).
35. H. Takayanagi *et al.*, Induction and activation of the transcription factor NFATc1 (NFAT2) integrate RANKL signaling in terminal differentiation of osteoclasts. *Dev. Cell* **3**, 889–901 (2002).
36. H. Kim *et al.*, Selective inhibition of RANK blocks osteoclast maturation and function and prevents bone loss in mice. *J. Clin. Invest.* **119**, 813–825 (2009).
37. I. R. Veland, A. Awan, L. B. Pedersen, B. K. Yoder, S. T. Christensen, Primary cilia and signaling pathways in mammalian development, health and disease. *Nephron Physiol.* **111**, 39–53 (2009).
38. V. Marion *et al.*, Transient ciliogenesis involving Bardet-Biedl syndrome proteins is a fundamental characteristic of adipogenic differentiation. *Proc. Natl. Acad. Sci. U.S.A.* **106**, 1820–1825 (2009).
39. W. Fu, P. Asp, B. Canter, B. D. Dynlacht, Primary cilia control hedgehog signaling during muscle differentiation and are deregulated in rhabdomyosarcoma. *Proc. Natl. Acad. Sci. U.S.A.* **111**, 9151–9156 (2014).
40. Z. Yao *et al.*, Tumor necrosis factor-alpha increases circulating osteoclast precursor numbers by promoting their proliferation and differentiation in the bone marrow through up-regulation of c-Fms expression. *J. Biol. Chem.* **281**, 11846–11855 (2006).
41. N. Kobayashi *et al.*, Segregation of TRAF6-mediated signaling pathways clarifies its role in osteoclastogenesis. *EMBO J.* **20**, 1271–1280 (2001).
42. J. Gohda *et al.*, RANK-mediated amplification of TRAF6 signaling leads to NFATc1 induction during osteoclastogenesis. *EMBO J.* **24**, 790–799 (2005).
43. V. Iotsova *et al.*, Osteopetrosis in mice lacking NF-kappaB1 and NF-kappaB2. *Nat. Med.* **3**, 1285–1289 (1997).
44. S. Takeshita *et al.*, SHIP-deficient mice are severely osteoporotic due to increased numbers of hyper-resorptive osteoclasts. *Nat. Med.* **8**, 943–949 (2002).
45. E. Purev, L. Neff, W. C. Horne, R. Baron, c-Cbl and Cbl-b act redundantly to protect osteoclasts from apoptosis and to displace HDAC6 from beta-tubulin, stabilizing microtubules and podosomes. *Mol. Biol. Cell* **20**, 4021–4030 (2009).
46. X. Yuan *et al.*, Ciliary IFT80 balances canonical versus non-canonical hedgehog signalling for osteoblast differentiation. *Nat. Commun.* **7**, 11024 (2016).
47. W. S. Chiu *et al.*, Transgenic mice that express Cre recombinase in osteoclasts. *Genesis* **39**, 178–185 (2004).
48. S. Yang, Y. P. Li, RGS12 is essential for RANKL-evoked signaling for terminal differentiation of osteoclasts in vitro. *J. Bone Miner. Res.* **22**, 45–54 (2007).
49. J. H. Jonason, R. J. O'Keefe, Isolation and culture of neonatal mouse calvarial osteoblasts. *Methods Mol. Biol.* **1130**, 295–305 (2014).
50. C. Itzstein, R. J. van 't Hof, Osteoclast formation in mouse co-cultures. *Methods Mol. Biol.* **816**, 177–186 (2012).
51. Y. P. Li, W. Chen, Y. Liang, E. Li, P. Stashenko, Atp6i-deficient mice exhibit severe osteopetrosis due to loss of osteoclast-mediated extracellular acidification. *Nat. Genet.* **23**, 447–451 (1999).
52. G. Yuan *et al.*, RGS12 is a novel critical NF-κB activator in inflammatory arthritis. *iScience* **23**, 101172 (2020).

Downloaded from https://www.pnas.org by TULANE UNIVERSITY RUDOLPH MATAS MED LIBRARY on June 23, 2022 from IP address 129.81.255.98.